



HAL
open science

Observation of selective optical manipulation of particles in acoustic levitation

Gabriel Dumy, Mauricio Hoyos, Jean-Luc Aider

► **To cite this version:**

Gabriel Dumy, Mauricio Hoyos, Jean-Luc Aider. Observation of selective optical manipulation of particles in acoustic levitation. *Journal of the Acoustical Society of America*, 2019, 146 (6), pp.4557-4568. 10.1121/1.5139640 . hal-03011089

HAL Id: hal-03011089

<https://hal.science/hal-03011089>

Submitted on 8 Dec 2020

HAL is a multi-disciplinary open access archive for the deposit and dissemination of scientific research documents, whether they are published or not. The documents may come from teaching and research institutions in France or abroad, or from public or private research centers.

L'archive ouverte pluridisciplinaire **HAL**, est destinée au dépôt et à la diffusion de documents scientifiques de niveau recherche, publiés ou non, émanant des établissements d'enseignement et de recherche français ou étrangers, des laboratoires publics ou privés.

Observation of selective optical manipulation of particles in acoustic levitation

Gabriel Dumy,^{1, a)} Mauricio Hoyos,^{1, b)} and Jean-Luc Aider^{1, c)}

*Physique et Mécanique des Milieux Hétérogènes, ESPCI Paris, PSL University,
CNRS, Sorbonne Université, Univ Paris Diderot, Sorbonne Paris Cité, 75005 Paris,
France*

1 Acoustic Radiation Force is commonly used to create stable large-scale aggregates of
2 particles in levitation (so-called "acoustic levitation") in a micro cavity. We show in
3 the following work that this well-known and well-controlled aggregation process can
4 be reversed without contact or external flow if the aggregated particles are enlight-
5 ened with the proper optical wavelength. This coupled optics and acoustics effect has
6 been observed with various kinds of particles and different optic wavelengths, show-
7 ing high reproducibility. The phenomenon is studied using fluorescent micro-metric
8 polystyrene particles without flow, and the effects of acoustic energy and illumina-
9 tion power have been quantitatively assessed. It is then exploited to separate a mix
10 of particles with identical mechanical properties, based on their different optic ab-
11 sorption. If the phenomenon is not well understood, we propose and discuss some
12 possible mechanisms that could be responsible for the rapid ejection of the objects in
13 levitation from the illuminated area. Since it is a tag free phenomenon which does not
14 need high energies to happen and since it works with biological objects such as algae,
15 red blood cells and bacteria, it may open the way to a broad range of applications.

a) gabriel.dumy@espci.fr; Also at : Paris Descartes, Sorbonne Paris Cité, Paris, France

b) mauricio.hoyos@espci.fr

c) jean-luc.aider@espci.fr

I. INTRODUCTION

Acoustic manipulation of micro-objects (particles, cells, bacteria, micro-bubbles, etc.) can be realized using ultrasonic standing waves in a fluidic or microfluidic resonator¹⁻⁴. Acoustic focusing of suspensions (or "acoustophoresis") is a complex phenomenon which has been the subject of many theoretical studies during the last decade. It occurs in a micro-channel or a micro-cavity when an acoustic wave of frequency f_{ac} , emitted into the cavity through a vibrating wall and reflected by the opposite wall, matches the resonance condition $\lambda_{ac} = 2h$, h being the height of the device (Fig. 1). In this case, particles such as plastic beads or living cells are drawn toward the acoustic pressure node created at mid-height of the cavity by the so-called Acoustic Radiation Force (ARF).

The ARF is the primary effect of the standing ultrasonic wave on the particles in suspension, and it rises from a second-order non-linearity. The ARF is different for each particle because it depends on their physical characteristics and size. The second effect of the ultrasonic standing wave is called acoustic streaming⁵⁻⁷. The acoustic wave transfers momentum to the fluid, leading to global motions of the particles through the Stokes force. The third effect is a Bjerknes force. It is basically a short distance force between particles⁸, attractive in most of the cases for the kind of particles used here, that contributes to the stabilization of the aggregate.

There are different theoretical models describing the ARF, based on more or less simplifying hypotheses⁹⁻¹⁵. King¹² was the first to propose computations on the forces on particles in a sound field based on several simplifying hypotheses. In particular, he considered the

37 particles as rigid spheres. In the following, we will use the Yosioka model¹³ which takes
 38 into account the compressibility of the spherical particles in the modeling. In this case, the
 39 primary Acoustic Radiation Force (ARF) F_{ac} responsible of particle acoustic levitation can
 40 be defined as:

$$\vec{F}_{ac} = \frac{\pi}{4} \langle E_{ac} \rangle k d_p^3 F_Y \sin(2 k_{ac} z) \vec{e}_z \quad (1)$$

41 where $\langle - \rangle$ denotes time averaging, d_p is the particle diameter, $\langle E_{ac} \rangle$ is the time-averaged
 42 acoustic energy density inside the channel, $k = \frac{2\pi}{\lambda_{ac}} = \frac{2\pi f_{ac}}{c}$ is the wave number of the
 43 acoustic plane wave of frequency f_{ac} , F_Y is the contrast factor, a positive (for polystyrene
 44 particles in water) numerical constant, and z is the axial (or vertical) position of the particle,
 45 $z = 0$ being at the bottom of the channel and $z = h$ being at the top of the channel (Fig. 1).
 46 The z axis also corresponds to the wave propagation direction.

47 The acoustic contrast factor of a given particle of density ρ_p in a medium of density ρ_f
 48 is defined as:

$$F_Y = \frac{1 + \frac{2}{3} \left(1 - \frac{\rho_f}{\rho_p}\right)}{2 + \frac{\rho_f}{\rho_p}} - \frac{\rho_f c_f^2}{3 \rho_p c_p^2} \quad (2)$$

49 where c_p is the speed of sound in the particles material and c_f is the speed of sound in the
 50 fluid. In this investigation we are dealing with an ultrasonic standing wave with a frequency
 51 $f_{ac} \sim 2$ MHz. The amplitude of the corresponding acoustic force typically ranges from 10^{-12}
 52 to 10^{-14} N. For instance, with polystyrene particles ($\rho_p = 1060$ kg.m⁻³, $c_p = 2350$ m.s⁻¹,
 53 $Z_{ps} = 2.5$ MPa.s.m⁻¹) dispersed in our resonator filled with water ($\rho_f = 1000$ kg.m⁻³,

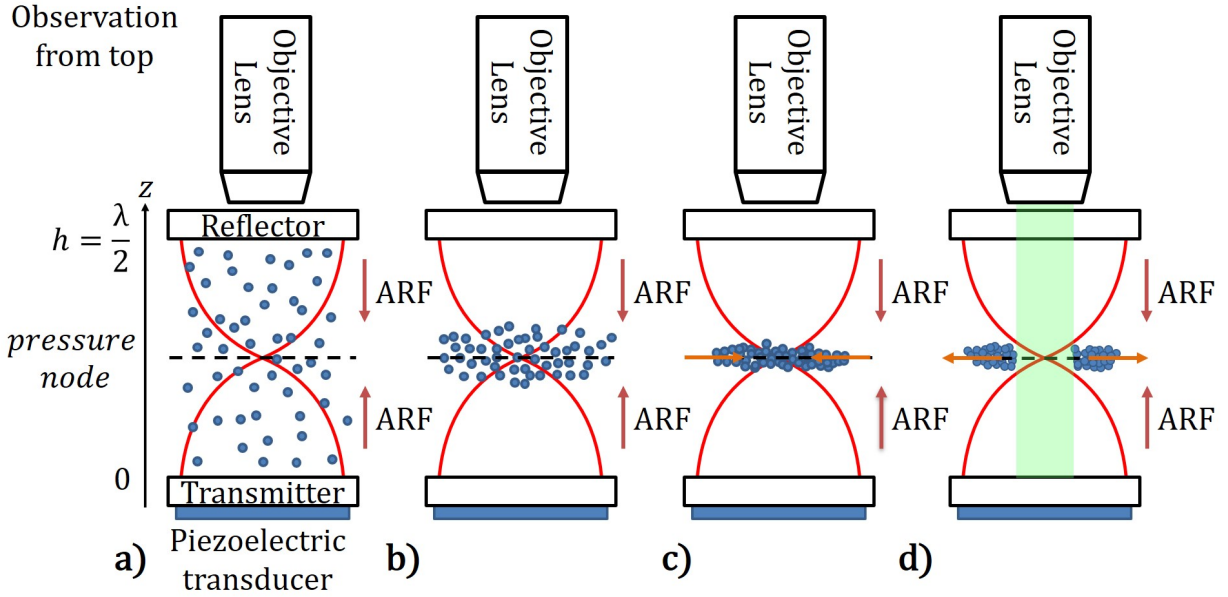


FIG. 1. (color online) Side view of an acoustic resonator showing the principle of acoustic focusing of a suspension of particles in an acoustic resonator (a, b) leading to the creation of an aggregate in acoustic levitation (c). Red lines denote the standing ultrasonic wave pressure profile. (d) The aggregate of fluorescent particles can then be broken up if illuminated with the proper optical wavelength, through the microscope internal light source.

54 $c_f = 1500 \text{ m.s}^{-1}$), F_Y equals 0.2244, and if particle diameter is $1 \mu\text{m}$, the primary acoustic
 55 radiation force equals $2.8 \times 10^{-13} \text{ N}$.

56 Once the particles have reached the nodal plane, the axial component of the force becomes
 57 null and the transverse component F_T is no longer negligible. Indeed it has been shown that
 58 this component is about one hundred times weaker than the axial component and is then

negligible during the focusing step^{16,17}. Whitworth¹⁸ derived the transverse component of
 the ARF for a radially symmetric acoustic wave in the nodal plane:

$$F_T = d_p^3 \frac{3(\rho_p - \rho_f)}{\rho_f + 2\rho_p} \nabla \langle E_{ac} \rangle \quad (3)$$

This transverse component depends directly on the radial gradient of the acoustic energy
 $\nabla \langle E_{ac} \rangle$ and is responsible for the aggregation of particles in the levitation plane toward the
 local maximum of acoustic energy, which are the final equilibrium positions that we observe.

After a short description of the experimental setup, we will present the first observa-
 tions of the ejection of particles in acoustic levitation when illuminated at specific optical
 wavelengths. The ejection velocity of the particles from the illuminated area is then stud-
 ied quantitatively, especially by varying the amplitude of the acoustic force field and the
 power of the light wave. The phenomenon is then applied to a binary mixture of particles,
 illustrating the great potential of this phenomenon as a new highly selective separation tech-
 nique. Finally the different possible mechanisms that could explain our observations and
 measurements are discussed, before coming to the conclusion.

II. MATERIALS AND METHODS

A. Acoustic resonator

In the following, all the experiments have been carried out in the same acoustic resonator
 whose dimensions are summarized on Fig. 2 a). We use a homemade aluminum circular
 cavity of diameter $D = 20$ mm and height $h = 400$ μ m. The cavity is closed by a round

77 quartz cover plate (reflector thickness $h_{ref} = 1.1$ mm) while the bottom is made of a
 78 silica wafer (transmitter thickness $h_{trans} = 0.30$ mm). The cover plate is easily removable
 79 and allows fast changes of the medium. The 2 MHz piezoelectric transducer (PZT) (square
 80 ceramic, 1 mm thick, 10 mm wide) is glued directly on the silica wafer using a water soluble
 81 glue. The PZT is powered by a wave generator (Tabor Electronics 5200) connected to an
 82 amplifier (Tabor Electronics 3222) allowing the variation of the applied voltage between
 83 a few mV to more than 10 V peak to peak. A correlation is made between the acoustic
 84 energy carried by the generated standing ultrasonic field and the voltage applied to the
 85 piezoelectric transducer, by measuring the axial focusing velocity $v_z(z)$ of a spherical bead,
 86 which is directly proportional to the acoustic energy. Using polystyrene spheres of known
 87 compressibility and density, we can find the acoustic energy density¹⁹. We will thus speak of
 88 acoustic energy when referring to the amplitude of the acoustic field in the remaining of the
 89 article. The frequency f_{ac} of the sinusoidal signal is tuned to maximize the acoustic radiation
 90 force which corresponds to the resonance condition $\lambda_{ac} = 2h$. We find this resonance
 91 by monitoring the reflected electric signal through an oscilloscope (LeCroy WaveAce 214),
 92 and minimizing the amplitude of said signal. In our case, the optimal frequency is $f_{ac} \simeq$
 93 1.85 MHz, but day-to-day fluctuations can occur, caused by small room temperature change,
 94 or slight errors in the position of the quartz cover plate. These fluctuations are on the order
 95 of $0.5\%f_{ac} \simeq 10$ kHz.

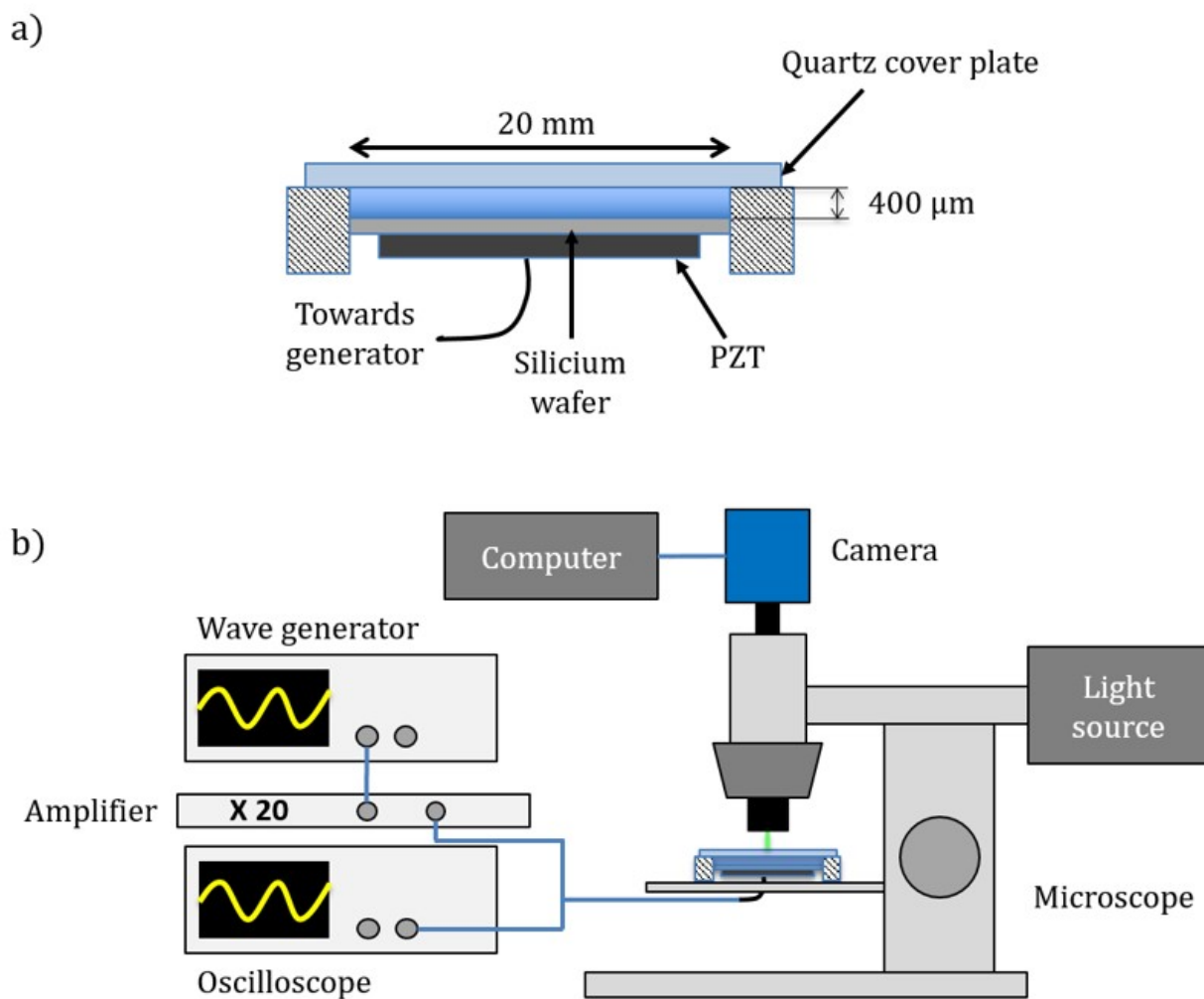


FIG. 2. (color online) a) Sketch of the acoustic resonator, showing the piezoelectric transducer (PZT) glued under a silicone wafer, establishing a standing acoustic field in the cavity above, enclosed by aluminum walls and a quartz top cover plate. b) Sketch of the experimental setup showing the acoustic generation devices, the acoustic resonator placed on the moving stage of a microscope.

96 **Optical setup**

97 The acoustic resonator described above was then placed on the moving stage of a fluores-
98 cence microscope (Olympus BX-2 and Olympus BXFM). The observations were made using
99 objectives with different magnification, depending on the size of the aggregates. The light
100 source for white light and fluorescence experiments is a LED source (CoolLED pE-300-W)
101 allowing a reasonably good control of the wavelength range and power of illumination. The
102 microscope is equipped with two filter cubes allowing the monitoring of the green or red
103 fluorescences. The filter 1 is centered on the Green Fluorescent Protein (GFP) range, i.e.
104 an excitation wavelength $\lambda_{abs} = 488$ nm and an emission wavelength $\lambda_{fluo} = 525$ nm,
105 while filter 2 is centered on *Discosoma* RED protein (DsRED) range, i.e. $\lambda_{abs} = 545$ nm
106 and an emission wavelength $\lambda_{fluo} = 620$ nm. Color movies presented here for qualita-
107 tive observations were recorded using a INFINITY3-3UR Lumenara camera at 50 fps. The
108 quantitative experiments were recorded using a PCO Dimax CS3 © fast camera at 100 fps.
109 The images resulting from experiments were post-treated with the free software ImageJ
110 (<https://imagej.nih.gov/ij/>), to adjust contrast, crop areas of interest and to produce
111 the spatio-temporal diagrams illustrated on Fig.6. The intensity delivered by the illumi-
112 nation lamp has been measured with a ThorLabs PM16-130 Probe (Spectral range 400 to
113 1100 nm, 1 cm \times 1 cm silicon sensor area, optical power range 5 pW - 500 mW) connected
114 to the same computer controlling the other instruments.

115 III. CREATION OF LARGE-SCALE AGGREGATES UNDER ACOUSTIC RADI- 116 ATION FORCE

117 As explained in the previous sections, the ARF is a simple and fast process to create
118 large aggregates of particles in acoustic levitation. Once the ultrasonic wave is generated
119 with the proper frequency into the cavity, the ARF forces the suspended particles to move
120 toward the nodal plane, at mid-height of the cavity. Once the particles have reached the
121 focusing plane, the transverse component of the ARF forces the particles to move toward
122 the location of the maximum of acoustic energy and then create an aggregate. When the
123 particles are close enough from each other then the Bjerknes force keep the particles close
124 together, making the aggregate more compact and stable. The creation of a large aggregate
125 of particles is illustrated on Fig. 3 a) with 1.62 μm polystyrene beads. The focusing time
126 T_{foc} can be very short (a few tenths of second), depending on the amplitude of the ARF.
127 Once the aggregate is formed, it can be kept in acoustic levitation as long as needed and
128 will remain stable, with the same spatial organization²⁰. The aggregation process is efficient
129 on particles as well as cells or active matter (bacteria). It can be used as a tool for creating
130 an acoustic trap, especially for self-propelled organisms like bacteria that can be held in
131 levitation in acoustic confinement²¹.

132 In previous works²⁰ we demonstrated that it is also possible to generate and sustain a
133 2D aggregate of particles using burst mode acoustic, or pulsed acoustic, i.e. applying a
134 low-frequency square wave modulation with a given duty-cycle. We also demonstrated that
135 it helps suppressing the acoustic streaming for particles smaller than 1 μm . It is also of great

136 help to control the amount of acoustic energy injected in the setup as well as limiting the
 137 possible thermal heating of the piezoelectric element when running long-time experiments,
 138 therefore reducing the potential thermal detuning of the resonator. It will be useful in the
 139 following to evaluate the possible influence of acoustic streaming on the phenomenon.

140 **IV. BREAKUP OF AGGREGATES**

141 As mentioned previously, once an aggregate of passive particles is formed using ARF,
 142 it remains stable and can be kept in levitation as long as needed. Without the use of an
 143 external flow or force, there is no way to break it up, apart from lowering enough or turning
 144 off the acoustics. In that case the aggregate either disintegrates in small aggregates and
 145 particles which all sediment, or the entire aggregate sediments, with particles still being
 146 stuck to each other by short distance hydrodynamic interactions.

147 There can be other behaviors with active matter, for instance when aggregating bacteria
 148 (active) or Janus particles (pseudo active). Indeed, when aggregated bacteria kept in levi-
 149 tation are released from the confinement imposed by the acoustic field, the aggregate inner
 150 active pressure triggers an explosion-like breakup, radially ejecting bacteria confined in the
 151 acoustic field²¹. In the case of Janus particles, as demonstrated by Takatori et al.²², the re-
 152 laxation of an active crystal has been observed and described when the acoustic confinement
 153 is released.

154 What we shall report in the following is a breakup process of aggregates of particles kept
 155 in acoustic levitation using specific illuminations.

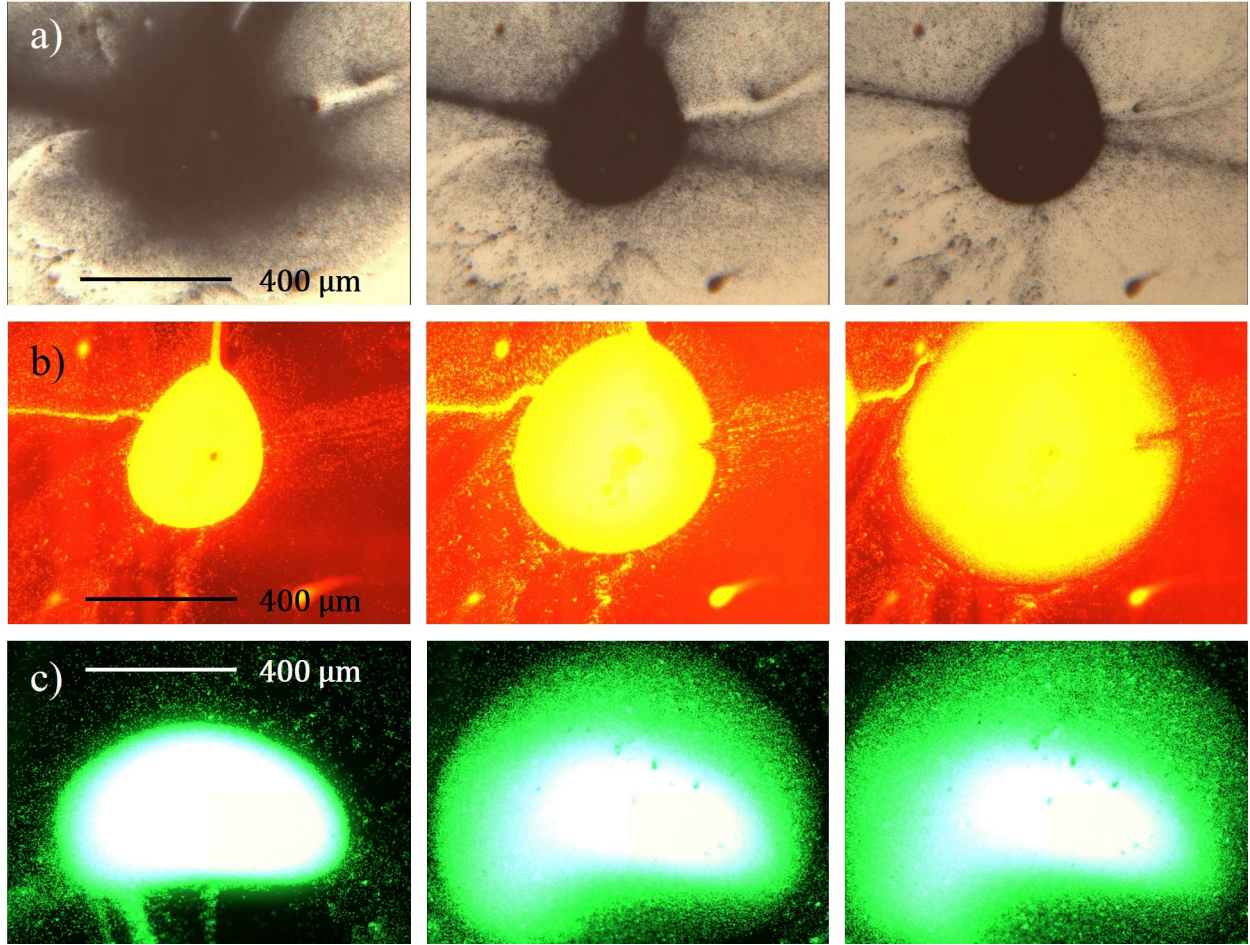


FIG. 3. (color online) Time steps between frames is 200 ms. a) The three first pictures show the formation of a large stable aggregate of $1.62 \mu\text{m}$ polystyrene particles under a $f_{ac} = 1.86 \text{ MHz}$ acoustic field. It can be kept stable as long as needed. b) When the same aggregate is illuminated with a green light ($\lambda_{light} = 545 \text{ nm}$) at a much higher intensity, the particles are quickly ejected from the illuminated region (see SI Movie 1). c) We observe the same phenomenon with $1.75 \mu\text{m}$ polystyrene particles fluorescing in green and illuminated with a blue ($\lambda_{light} = 488 \text{ nm}$) light at the same intensity (see SI Movie 2).

156 **V. BREAKUP OF AGGREGATES OF FLUORESCENT PARTICLES BY LIGHT**157 **A. First observations**

158 We use fluorescent polystyrene particles of diameter $d_p = 1.62 \mu\text{m}$ which can be excited
159 with green light and fluoresce in red light ($\lambda_{abs} = 545 \text{ nm}$ and $\lambda_{em} = 620 \text{ nm}$). Large
160 aggregates of particles are created in acoustic levitation in the cylindrical resonator described
161 on Fig. 2 using $f_{ac} = 1.86 \text{ MHz}$ resonant frequency. As mentioned previously, the aggregates
162 can be kept stable as long as needed when observed with a white light and at standard
163 microscope illumination power, below $5 \text{ mW}\cdot\text{mm}^{-2}$ (The regular aggregation process can be
164 seen in Fig. 3 a)).

165 Interestingly, when using a monochromatic ($\lambda = 545 \text{ nm}$) illumination, and gradually
166 increasing the light intensity, the aggregation process is stopped. For even higher intensities,
167 the aggregate starts to eject particles from its periphery. This ejection process goes on until
168 disruption of the entire aggregate. If the light intensity is still increased, then this ejection
169 process takes the form of an explosion, as can be seen on Fig. 3 b) and associated movie
170 (see SI Movie 1, 4). One astonishing effect is that the particles escape the aggregate while
171 remaining in the focal plane of the camera, i.e. in levitation. This result suggests that
172 the primary radiation force (responsible for the acoustic focusing) is not affected, but that
173 transversal and Bjerknes forces seems to be completely counterbalanced or screened by
174 another force.

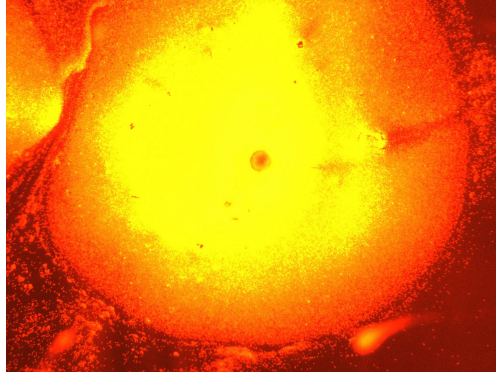


FIG. 4. Movie (MM1) showing the formation of an aggregate made of $1.62\ \mu\text{m}$ beads under the influence of a $1.86\ \text{MHz}$ acoustic field. This aggregate is then disrupted when illuminated with a high intensity monochromatic green light. As soon as the standard white illumination is restored the aggregate recovers its initial shape.

175 MM.1. Observation of the standard process of formation of an aggregate in acoustic lev-
 176 itation. It is then disrupted under monochromatic illumination. The aggregate is reformed
 177 quickly when the white light illumination is restored. This is a file of type “mp4” (4.5 Mb)

178 The disaggregation only occurs in acoustic levitation (no effect observed on beads that are
 179 on the bottom or top of the cavity) and when the particles are illuminated with the proper
 180 wavelength corresponding to the fluorescent particle absorption wavelength. In this case, for
 181 instance, the aggregate remains unchanged if illuminated with a blue light ($\lambda = 488\ \text{nm}$).

182 Another interesting point is that the effect is reversible: once the light intensity is lowered
 183 under a given threshold, then the standard acoustic aggregation process starts again with
 184 the same dynamics (as demonstrated at the end of SI Movie 1).

185 This phenomenon is highly reproducible and not limited to a given type of fluorescent
 186 bead. It has been tested with various fluorescent particles, all experiments leading to the

187 same observations. Another example is shown Fig. 3 c), where an aggregate made from a
 188 solution of particles of diameter $d_p = 1.75 \mu\text{m}$ which can be excited with blue light and
 189 fluoresce in green light ($\lambda_{abs} = 450 \text{ nm}$ and $\lambda_{em} = 532 \text{ nm}$) is formed under an acoustic
 190 field of frequency $f_{ac} = 1.85 \text{ MHz}$. As soon as we illuminate this aggregate with a blue light
 191 ($\lambda = 488 \text{ nm}$ at $50 \text{ mW}\cdot\text{mm}^{-2}$), the aggregate starts to eject particles from its periphery, as
 192 was observed before (see SI Movie 2, 5). The same expulsion phenomenon could be observed
 193 in a very reproducible way using these different fluorescences and with various diameters d_p ,
 194 ranging from 0.883 to $5 \mu\text{m}$, when the aggregate was illuminated with the right wavelength.

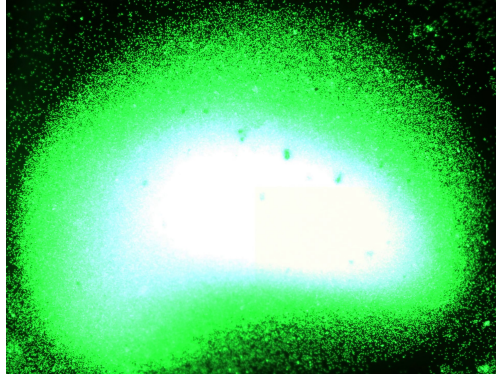


FIG. 5. Movie (MM2) showing the disruption of an aggregate made of $1.75 \mu\text{m}$ beads under the influence of a 1.85 MHz acoustic field, illuminated by a strong blue light.

195 MM.2. Disruption of an aggregate made of green fluorescent $1.75 \mu\text{m}$ polystyrene beads.
 196 This is a file of type “m4v” (4.1 Mb)

197 **B. Influence of the light intensity**

198 As mentioned in the previous section, one can find a critical illumination intensity I_{crit}
 199 for which the acoustic radiation force and the opto-acoustic force seem to balance each

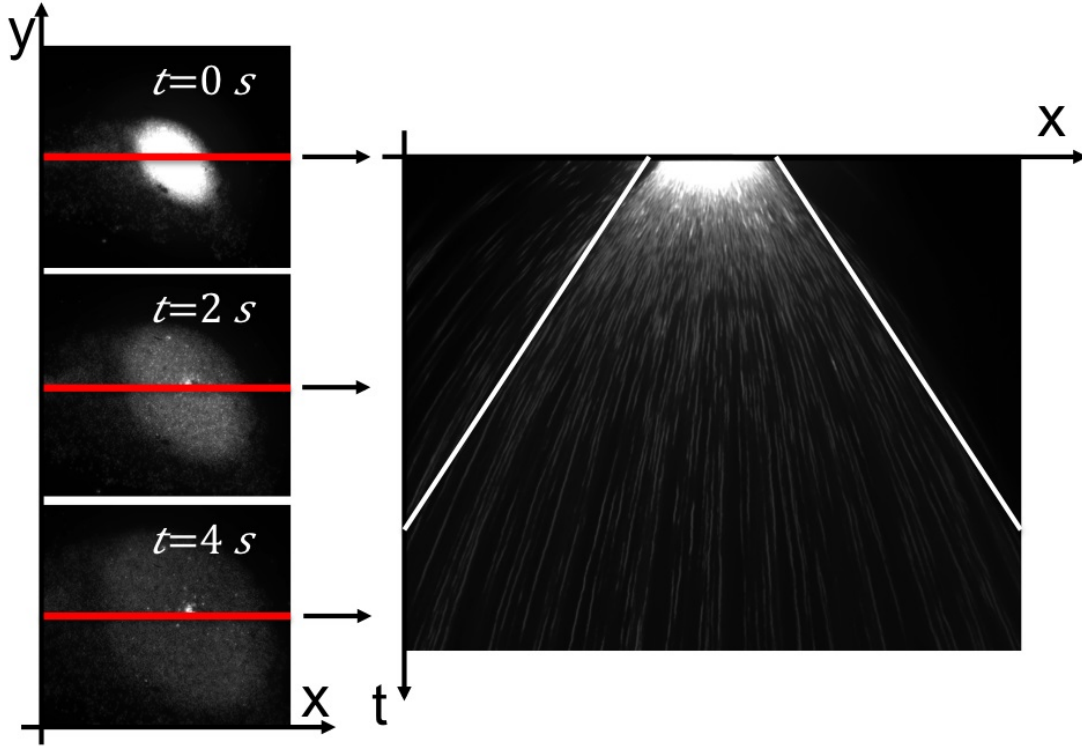


FIG. 6. Principle for spatio-temporal analysis. A given line across an aggregate is chosen and plotted as a function of time. The resulting picture gives an overall view of the expulsion process. The ejection velocity is then measured as the slope of the cone frontier in the spatio-temporal diagram.

200 other. To further investigate the dependence of the effect on the amount of light injected in
 201 the aggregate, we did vary the light intensity for a given aggregate of $1.62 \mu\text{m}$ beads, at a
 202 fixed amplitude of the acoustic field ($f_{ac} = 1.85 \text{ MHz}$). In the following the amplitude of
 203 the acoustic force is considered proportional to the acoustic energy inside the resonator (cf.
 204 Eq. 1). In this case, this energy is constant ($\langle E_{ac} \rangle = 10 \text{ J.m}^{-3}$).

205 To quantify the disaggregation dynamics, we use spatio-temporal diagrams as explained
 206 in Fig. 6. A line crossing the stable aggregate is chosen before illumination. The aggregate

207 being a bright spot over a dark background, the line crossing it shows a clear frontier between
 208 the aggregate and surrounding fluid. The time-evolution of these lines is then plotted as a
 209 function of time, leading to a spatio-temporal diagram (left part of Fig. 6). The disruption
 210 of the aggregate is then visualized as a cone in the spatio-temporal diagram. The slope of
 211 the cone frontier in the spatio-temporal diagram leads directly to the expulsion velocity v_{ej} .

212 It is then possible to measure the ejection velocity for each illuminations. The evolution
 213 of v_{ej} as a function of the illumination power P_{light} is plotted on Fig. 7 a). A linear evolu-
 214 tion is found suggesting a direct proportionality of the ejection velocity with the injected
 215 illumination power: $v_{ej}(P_{light}) \propto P_{light}$.

216 C. Influence of the amplitude of the ARF

217 Similarly, the influence of the acoustic force amplitude has been investigated. We also
 218 found that the phenomenon was no longer observed when the acoustic field is turned off.
 219 This time, we did explore a range of ARF amplitudes ranging from 8 to 200 J.m^{-3} at
 220 $f_{ac} = 1.85 \text{ MHz}$ for a given illumination power (50 mW.mm^{-2}), all other parameters being
 221 kept constant.

222 Using the same spatio-temporal analysis, we plot on Fig. 7 b) on logarithmic scale the
 223 evolution of v_{ej} as a function of the acoustic energy in J.m^{-3} for a given illumination power
 224 P_{light} . In this case, a linear evolution is found suggesting a scaling of the ejection velocity
 225 as a 3/4 power law of the acoustic energy: $v_{ej}(\langle E_{ac} \rangle) \propto \langle E_{ac} \rangle^{3/4}$. Combining both results,
 226 and considering that both parameters are independent, one can define the following scaling
 227 law for the ejection velocity: $v_{ej}(P_{light}, \langle E_{ac} \rangle) \propto P_{light} \cdot \langle E_{ac} \rangle^{3/4}$.

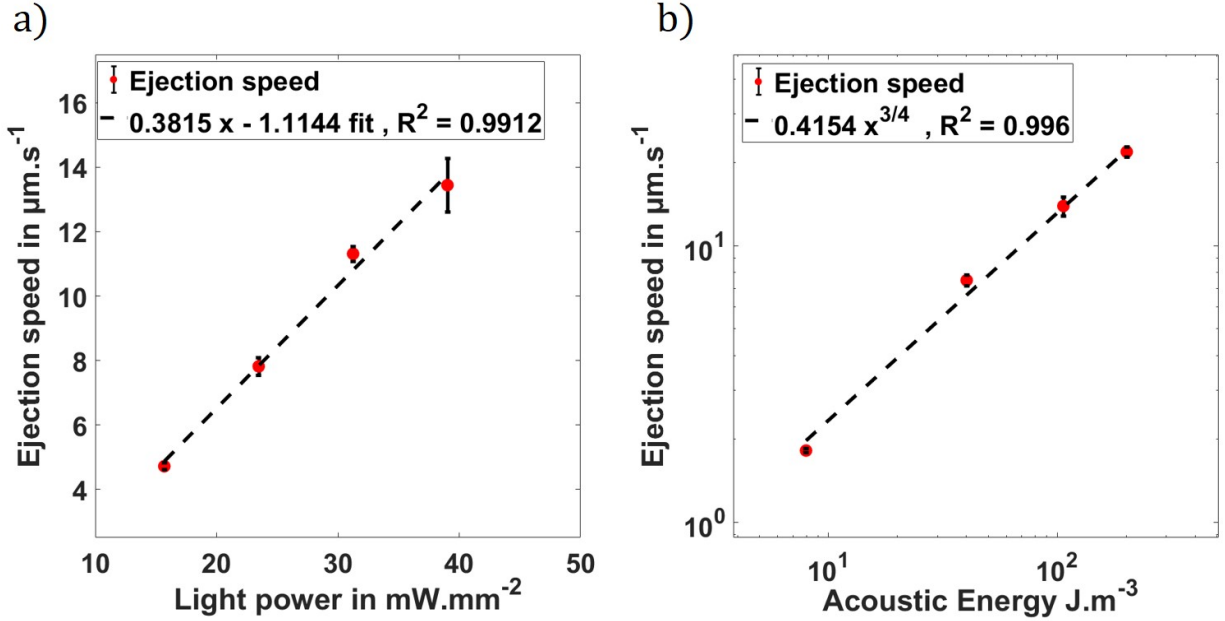


FIG. 7. Evolution of the ejection velocity as a function of the illumination power (constant $\langle E_{ac} \rangle = 106 \text{ J}\cdot\text{m}^{-3}$) (a) or of the amplitude of the ARF (constant illumination power of $50 \text{ mW}\cdot\text{mm}^{-2}$) (b) for a given suspension of $r_p = 1.62 \text{ }\mu\text{m}$ polymer beads under the influence of a $f_{ac} = 1.85 \text{ MHz}$ acoustic field.

228 D. Influence of acoustic streaming

229 Acoustic streaming is a common phenomenon when using standing acoustic waves in
 230 resonant cavities. It could be considered as a possible explanation for the breakups of the
 231 aggregates, so we did investigate this effect.

232 As briefly described in section III, it is possible to control the onset of acoustic streaming
 233 in our resonators using a burst signal. The duty cycle DC of the ultrasonic wave can be

234 defined as the ratio between the time when the ultrasounds are emitted over the total period
 235 of the excitation :

$$DC = \frac{T_{ON}}{T_{OFF} + T_{ON}} \quad (4)$$

236 When we vary this parameter, we are modifying the temporal average of the acoustic en-
 237 ergy that plays a role in the ARF. Fig. 8 represents the ejection speed of 1.62 μm polystyrene
 238 particles, when submitted to a 1.908 MHz ultrasonic standing field, with an acoustic energy
 239 of 160 J.m^{-3} , and enlightened with a light power of 50 mW.mm^{-2} . The acoustic field is
 240 then modulated by a square signal of period $T_{burst} = 1 \text{ ms}$, and we then vary the duty
 241 cycle of the resulting field. As can be seen on this figure, at low duty cycles, we observe a
 242 linear evolution of the ejection speed with an increase of the duty cycle.

243 Defining a threshold for the acoustic streaming²³ (below which no acoustic streaming
 244 is affecting the aggregates in levitation), we can find a critical duty cycle for these burst
 245 parameters, that is represented by a gray bar on Fig. 8. Below this threshold, we do not
 246 observe any streaming in the cavity²⁰. Interestingly enough, when we cross the acoustic
 247 streaming threshold, we do not observe any change in the evolution of the ejection velocity.
 248 The fact that we do observe breakups of aggregates, with the same coupling between acoustic
 249 energy and light power below its threshold means that the origin of this phenomenon is not
 250 acoustic streaming.

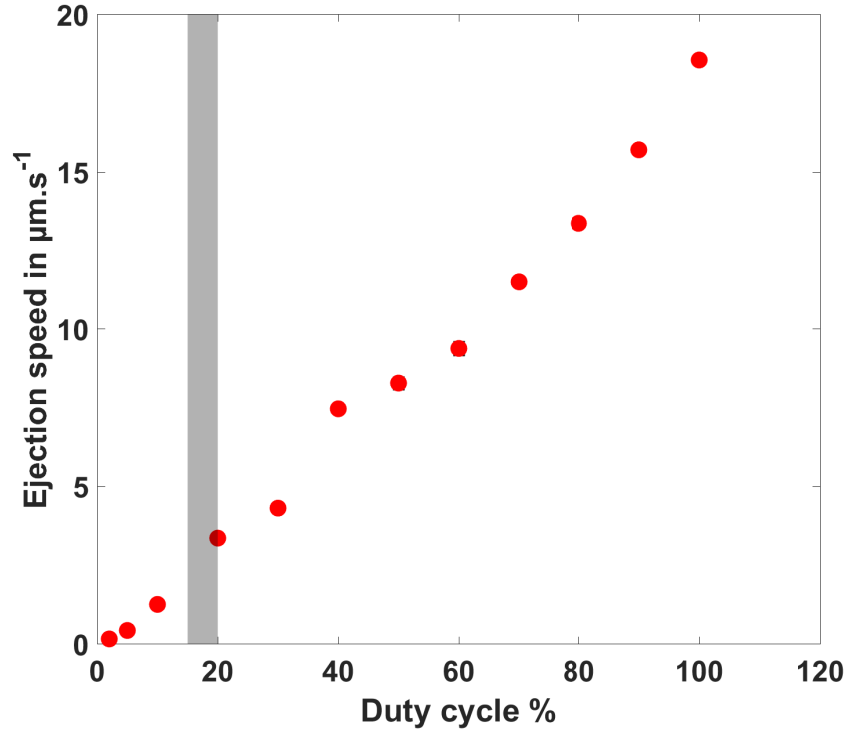


FIG. 8. Influence of the duty cycle on the ejection speed. The grey bar indicates the critical duty cycle below which we do not observe acoustic streaming. Error bars are smaller than the dots size.

251 **VI. SEPARATION OF A BINARY MIXTURE**

252 To demonstrate the ability of the opto-acoustic effect to separate a binary mixture, we
 253 used a mixed solution of two colloidal particles: polystyrene particles of mean diameters
 254 $d_{p1} = 1.62 \mu\text{m}$ and $d_{p2} = 0.883 \mu\text{m}$, with absorption wavelengths $\lambda_1 = 532 \text{ nm}$ and
 255 $\lambda_2 = 450 \text{ nm}$ with an equal volume fraction of 0.025 %. First we created a large ag-
 256 gregate in acoustic levitation, following the same process as in the previous experiments
 257 (1.903 MHz and 200 J.m^{-3}) and using the same resonator. After a relatively short focus-
 258 ing time, the aggregate becomes stable in acoustic levitation. The aggregate contains an
 259 homogeneous mixture of both particles.

260 The upper row of Fig. 9 shows the aggregates in acoustic levitation but using different
261 filters. Fig. 9 a) corresponds to an observation without filters. It shows a large aggregate in
262 stable acoustic levitation. When using a green (Fig. 9 b) or red filter (Fig. 9 c) one can see
263 that both types of particles are rather homogeneously distributed over the entire aggregate.
264 To our knowledge, it is impossible to separate such a mixture of particles once they are so
265 well mixed using acoustics alone.

266 The aggregate has then been illuminated with a blue light ($\lambda_{light} = 488 \text{ nm}$) at a constant
267 power of $30 \text{ mW}\cdot\text{mm}^{-2}$ during 10 seconds, then the illumination has been turned off. The
268 resulting aggregate has then been observed once the particles have aggregated again under
269 the influence of ARF. The result is shown on the lower part of Fig. 9. Fig. 9 d) shows
270 the aggregate after a few seconds without any optical excitation. One can see that the
271 aggregate has changed from its original shape. Fig. 9 e) and Fig. 9 f) shows the pictures
272 of the aggregate when observed respectively with a green and red filter. We can clearly see
273 that the aggregate no longer contains an homogeneous mixture of both particles. The red
274 fluorescent beads are now on one side of the aggregate while the green are now on the other
275 side of the aggregate. This is a clear demonstration that the two types of particles have
276 indeed been separated by the photoacoustofluidic effect. The separation was very fast (a
277 few seconds) and efficient. The particles absorbing the illumination wavelength (the smaller
278 ones in this case) have indeed been extracted from the aggregate before being attracted
279 again toward the aggregate of larger particles, which did not breakup, because of the ARF.

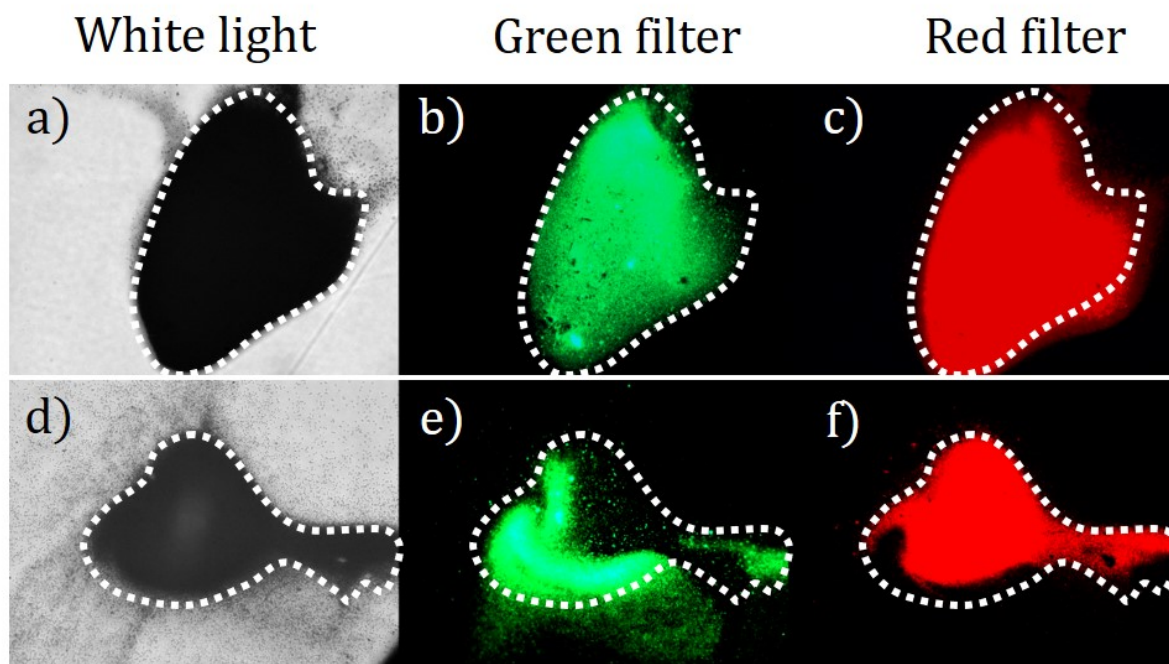


FIG. 9. (color online) Separation of a binary mixture of $1.62 \mu\text{m}$ red fluorescent particles, and $0.883 \mu\text{m}$ green fluorescent particles. a), b) and c) pictures show the stable aggregate created by the acoustic force. The three pictures corresponds to observations without selective filter (a) and with respectively green (b) and red (c) filters. The pictures d), e) and f) show the aggregate after applying a strong illumination to the green fluorescent particles during 10 seconds and after all the ejected particles had time to focus again toward the aggregate. One can see that the new aggregate is no longer an homogeneous mixture of the two types of particles. It is now made of two clearly separate regions: one containing the red particles, the other one containing the green particles.

280 VII. DISCUSSION

281 A. Coupled dependency on acoustic and illumination

282 The previous experiments show a clear correlation between acoustics energy and illumi-
 283 nation power for the breakdown of aggregates. To evaluate this coupling, we studied the
 284 evolution of the ejection speed from the aggregates when varying the illumination power
 285 and amplitude of the ARF for a given suspension of particles ($d_p = 1.62 \mu\text{m}$). The result
 286 is shown on Fig. 10 as a phase diagram: we represent the initial ejection speed of particles
 287 from the aggregate as a function of illumination power and acoustic energy applied to the
 288 aggregate, i.e. a contour plot of $v_{ej}(P_{light}, \langle E_{ac} \rangle)$, the color bar being proportional to v_{ej} .
 289 The $1 \mu\text{m}\cdot\text{s}^{-1}$ speed contour line is highlighted in red, and corresponds to the Brownian mo-
 290 tion speed at experiment temperature (20 degrees Celsius) for these particles and has been
 291 identified as the threshold between stable aggregate and aggregate breakup zones. As one
 292 can observe, the aggregate is locked in a stable state, provided that the illumination power
 293 is below $10 \text{ mW}\cdot\text{mm}^{-2}$, or the acoustic energy of the ultrasound field is below $25 \text{ J}\cdot\text{m}^{-3}$.
 294 Once this threshold is crossed (solid red line on the phase diagram, corresponding to the
 295 Brownian motion at the experiment temperature, for these particles), then we have a more
 296 or less linear evolution of the ejection speed as light power or acoustic energy is increased.
 297 Interestingly, there seem to be a threshold on acoustic energy density at $160 \text{ J}\cdot\text{m}^{-3}$, above
 298 which the light dependence of the ejection speed changes. It seems to be an optimum on illu-
 299 mination power dependence, as it is the point where the highest ejection speeds are reached
 300 using the lowest illumination power. After this threshold, we need to put more illumination

301 power to reach the same ejection speed. One possible explanation for this behavior is that
 302 for these high acoustic energies, the acoustic streaming is no longer negligible, and may
 303 interact with the expulsion process, leading to some errors in the estimation of the initial
 304 ejection velocity (leading to a no longer isotropic ejection).

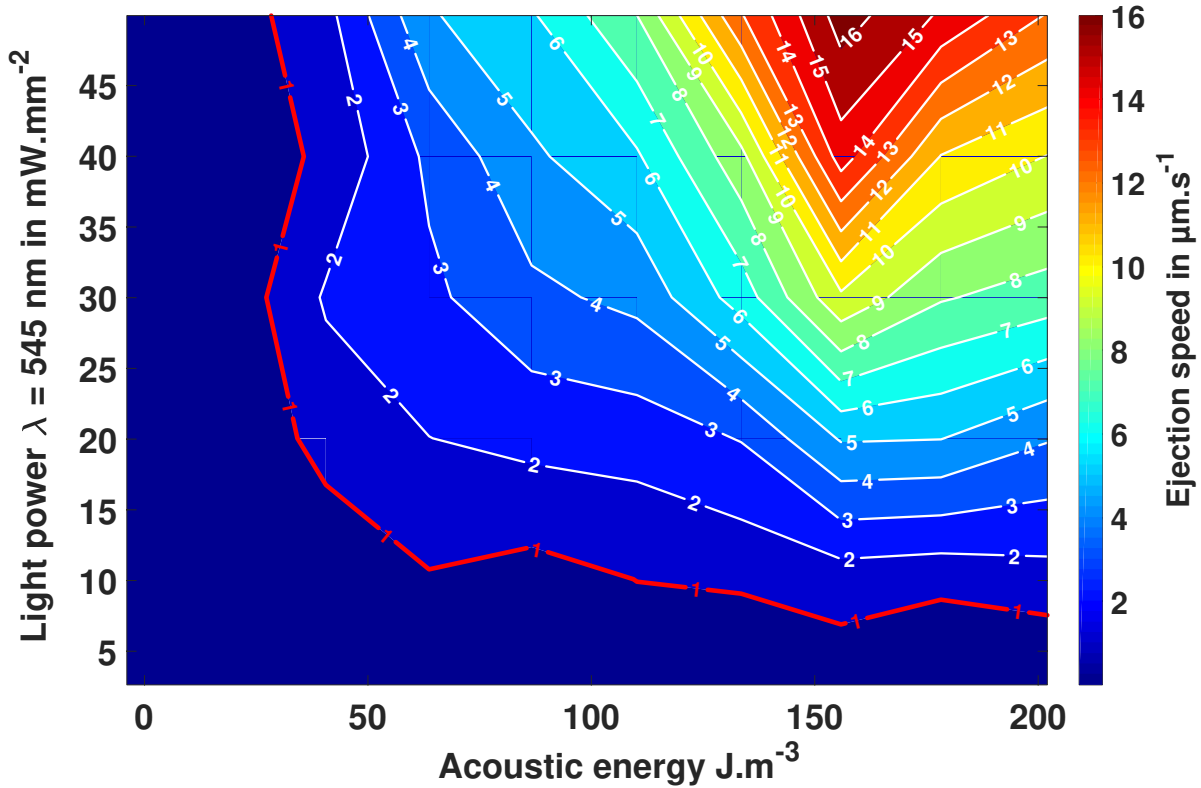


FIG. 10. (color online) Determination of the phase diagram for an assembly of $1.62 \mu\text{m}$ red fluorescent particles. The ejection speed of particles from the aggregate are represented with a color scale, against the power of the light used on the aggregate and the squared voltage applied to the piezoelectric ceramic, representing the acoustic energy inside the resonator. The $1 \mu\text{m.s}^{-1}$ speed contour is the thermal agitation speed at experiment temperature (20 degrees Celsius) and has been identified as the threshold between stable aggregate and aggregate breakup zones.

305 These results show that both acoustic and light excitation are needed to observe this
 306 phenomenon. Particles need to absorb light at the specific optic excitation wavelength used
 307 to be ejected from the aggregates, and to be trapped at the same time in an acoustic field
 308 carrying enough acoustic energy. This means that the optic energy absorbed by the particles
 309 needs to play a role in the explanation of the phenomenon.

310 **B. Influence of heating on particles properties**

311 The most plausible explanation is that optical illumination at specific wavelength leads to
 312 absorption and conversion of incident light (E_λ) into thermal heating. One basic explanation
 313 could be that while absorbing light, particles heat up, thus modifying their mechanical
 314 properties, potentially affecting the sign of the acoustic contrast factor in Eq. 2. However,
 315 after calculation, compressibility and density of polystyrene and water do not change that
 316 much between 20 and 100 degrees Celsius. Moreover, if the acoustic contrast factor were to
 317 change sign, then the principal component of the ARF (responsible for the vertical focusing
 318 of the particles) would also be affected, and we do not observe a movement out of the focal
 319 plane.

320 **C. Heating of the fluid itself**

321 One could argue that it is the fluid itself that heats up when exposed to a strong illumi-
 322 nation, under the confinement of the acoustic field. Having the fluid directly react to the
 323 coupled excitation could then create a large scale flow dragging away the particles. To try
 324 this, we have performed experiments using coloured beads. Two types of particles having

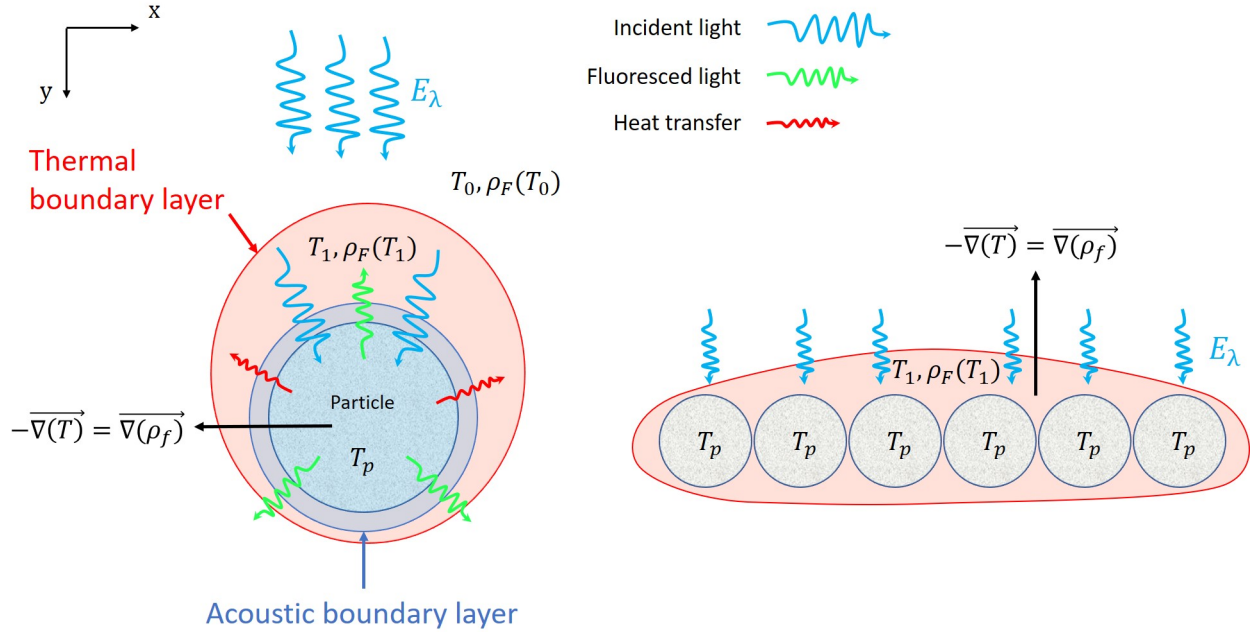


FIG. 11. (color online) Illustration of how the particle (or an aggregate, as depicted on the right side of the graphic) once illuminated by an optical wave might heat up the surrounding liquid, thus generating an asymmetrical thermal layer around it, which might generate motion by convection or acoustic instability.

325 the exact same mechanical properties (same radii = 10 μm , made of polystyrene), in the
 326 same acoustic field ($\langle E_{ac} \rangle = 106 \text{ J.m}^{-3}$, $f_{ac} = 1.90 \text{ MHz}$), have been illuminated with
 327 the same optical wave ($\lambda = 550 \text{ nm}$ or 580 nm , $P = 50 \text{ mW.mm}^{-2}$). The only difference
 328 between the two populations was their optical absorption, one of the particle type being red-
 329 dyed while the other was transparent (plain polystyrene). Everything else being equal, the
 330 acoustic force is the same on the two species. When illuminated with the same wavelength
 331 and power, the dyed particles are almost instantly dispersed, while the transparent ones are
 332 not affected by the light (see SI Movie 3, 12). That confirms that the particles need only

333 absorbing the illumination wavelength and that they are the source of the phenomenon, and
 334 not the fluid itself.

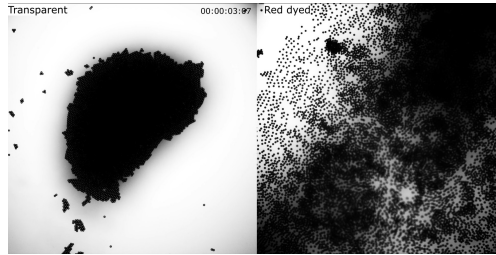


FIG. 12. Movie (MM3) Side to side comparison of the evolution of (left) an aggregate of plain polystyrene particles being 10 μm in diameter, and (right) the same particles red-dyed. They are both confined in the same acoustic field ($\langle E_{ac} \rangle = 106 \text{ J.m}^{-3}$, $f_{ac} = 1.90 \text{ MHz}$) and enlightened with the same optical wave (580 nm, $P=50 \text{ mW.mm}^{-2}$). As the aggregate made of dyed particles is instantly dispersed, nothing happens to the particles that do not absorb the optical wave.

335 MM.3. Side to side comparison of an aggregate of plain polystyrene particles and another
 336 one being red dyed, under the same acoustic confinement and optical illumination. This is
 337 a file of type “mp4” (6.3 Mb)

338 D. Soret effect

339 Another effect that could affect the stability of the aggregate in acoustic levitation is
 340 related to the Soret effect, or Ludwig-Soret effect²⁵, or thermodiffusion, namely, particle mi-
 341 gration under temperature gradients. The Soret coefficient is the ratio between the thermal
 342 diffusion coefficient and the molecular coefficient of colloidal objects suspended in a liquid.
 343 The Soret coefficient is well understood in gases when molecules of different size differentially

344 migrate under a thermal gradient. Nevertheless, Soret effect is visible and measurable in
345 suspensions of polymers in organic solvents, but the theoretical models are still poorly devel-
346 oped. Concerning Soret effect of non colloidal particles (10 μm) in water, to our knowledge
347 only one study has been undertaken²⁵. The thermophoretic mobility of 10 μm polystyrene
348 particles has been estimated in water, in a thermal gradient corresponding to $0.25^\circ\text{C}/\mu\text{m}$,
349 yielding to a migration velocity of 5 $\mu\text{m}/\text{s}$. In our case, the red fluorescent particles being
350 1.62 μm in diameter, 10 μm is a good approximation of our thermal layer thickness. Having
351 even a few additional degrees in the aggregate will yield thermal gradients on this order of
352 magnitude. At the periphery of the aggregate, particles could be pushed away by a Soret-like
353 effect. When illuminated, the temperature in the aggregate is higher than that in the sur-
354 rounding liquid. With a Soret effect of non-colloidal species, particles migrate from higher
355 to lower temperatures, in qualitative agreement with our observations. Once particles are
356 far apart from each other, with distances longer than the Bjerknes acoustic forces range^{26,27},
357 the aggregate starts to disrupt. Unfortunately, thorough investigations would be needed to
358 precisely quantify the thermal gradient generated in the boundary layer surrounding the
359 particles in levitation and illuminated with the proper wavelength.

360 **E. A thermal boundary fluid layer**

361 Nevertheless, another thermal effect may originates from the heating of a layer of fluid
362 directly surrounding the particles, leading to a local change in the fluid properties this time.
363 It would create around the particle a soft shell-like boundary layer, reminding the results
364 obtained by Yasuda and Kamakura²⁸. While in their work magnitude of forces are discussed,

365 we believe such shell could lead to a different direction of the force. As shown on Fig. 11,
 366 it is probable that the local increase of the temperature on the upper part of the particles
 367 leads to a local increase of the temperature of the fluid layer close to the particle. This
 368 would lead to a local change of the fluid density around the particles. A "convection-like"
 369 instability could be triggered with a decrease of the fluid density which would then lead to
 370 an upward motion to the fluid layer. We did not observe an axial motion of the particles.
 371 It would be possible that the axial motion is stopped by the much stronger axial radiation
 372 force (justifying the acoustic coupling), leading to a lateral escape motion of the fluid layer,
 373 dragging the particles while staying in the levitation plane.

374 **F. Acoustic instability of the thermal boundary layer**

375 It has been shown recently that fluid layers with even a relatively small contrast factor
 376 can undergo ARF effects²⁴. This is a side effect that can be a strong limitation to the
 377 separation of species if they are transported in different layers of fluid of different densities.
 378 If the temperature of a particle T_{part} is different from the one of the surrounding fluid then
 379 a thermal boundary layer δ_{therm} is created around the particle, or around an aggregate of
 380 particles (See Fig. 11). It is then possible that there exist a fluid layer with a density
 381 $\rho_f(T_1)$ lower than the one of the surrounding fluid $\rho_f(T_0)$. Gradients of fluid density $\nabla\rho_f$
 382 will appear, leading to the following expression for the volume force F_{ac-flu} exerted on the

383 fluid (we denote $\hat{\rho}_f$ the dimensionless perturbation in the density, following the analytical
 384 development stated above²⁴) :

$$F_{ac-flu} = -\cos(2ky)E_{ac}\nabla\hat{\rho}_f \quad (5)$$

385 One can see that if there is density gradient, then the fluid layer will undergo an acoustic
 386 force aligned with density gradients, leading to a possible motion of the fluid layer. It
 387 may be that this fluid layer drags particle alongs, while these ones are still subject to the
 388 axial acoustic force (much larger than the lateral one), thus moving sideways. The resulting
 389 ejection speed would then be a competition between the transverse component of the acoustic
 390 force and the viscous drag imposed by this fluid layer. The scaling in this case would be
 391 interesting, since as described in Eq. 3 the lateral acoustic force scales with d_p^3 , and the drag
 392 at this R_e would scale with d_p only.

393 G. Heating process and size

394 If the motion origin is indeed related to an instability, either thermal or acoustic, of the
 395 surrounding fluid layer, one could expect that the effect will be weaker for larger particles.
 396 Indeed, the thickness of the thermal boundary layer will be the same, if all parameters are
 397 kept constant apart from the radius of the particle. The ratio δ_{ac}/r_p will decrease and the
 398 entrainment of the particles will become weaker.

399 We carried out preliminary experiments with a given type of fluorescent beads, made
 400 from the same material (polystyrene, green fluorescent), trapped in the same acoustic field
 401 ($\langle E_{ac} \rangle = 106 \text{ J.m}^{-3}$ for a frequency of $f_{ac} = 1.90 \text{ MHz}$) and illuminated with the same

402 optical wave (488 nm with a power of $50 \text{ mW}\cdot\text{mm}^{-2}$), but with three different diameters.
 403 We observed a reduction of the ejection velocity when increasing particle diameter, as can
 404 be seen on Fig. 13. The aggregate made of $1 \mu\text{m}$ particles undergoes the expansion effect,
 405 as described before. But this effect is less noticeable on the $3 \mu\text{m}$ particles aggregate after
 406 the same exposition time, and the $10 \mu\text{m}$ aggregate seems not to have been affected at all
 407 after the same manipulation. This result can be considered as a first hint of a possible
 408 mechanism associated to the heated fluid layer surrounding the particle. However, it could
 409 also stem from a competition between a fluid drag and the transverse component of the
 410 ARF as denoted in VII F.

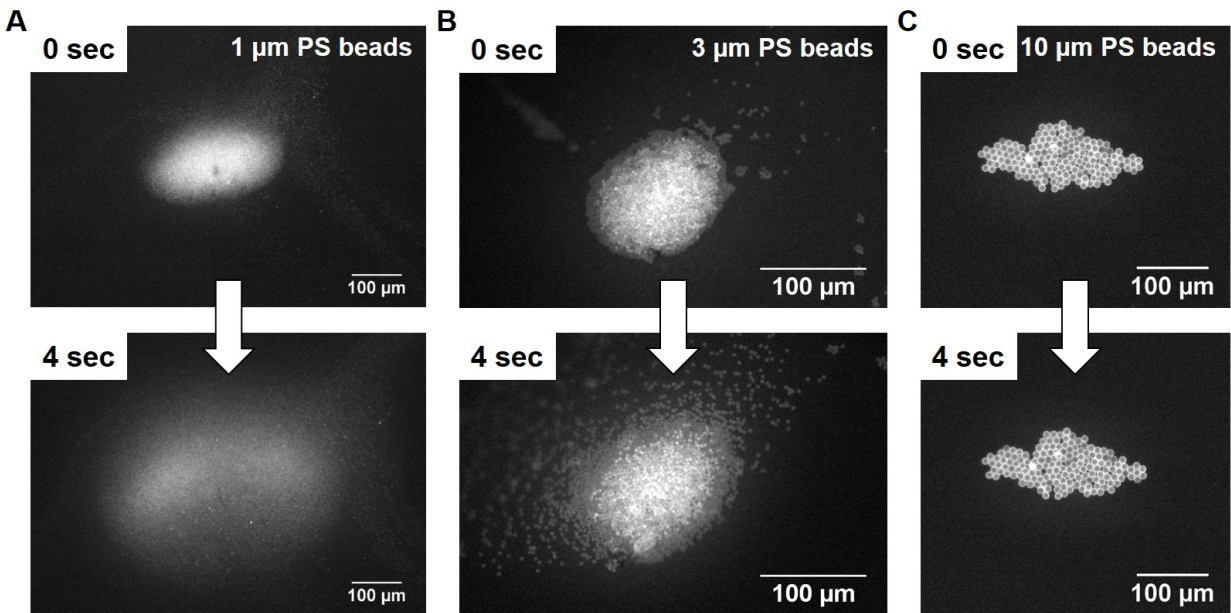


FIG. 13. Evolution of the aggregate behavior in acoustic levitation under illumination for different particle diameters, every other parameters being kept constant. The particles were green fluorescent polystyrene beads of various diameters, illumination was done at 488 nm with a power of $50 \text{ mW}\cdot\text{mm}^{-2}$, acoustic energy density was $\langle E_{ac} \rangle = 106 \text{ J}\cdot\text{m}^{-3}$ for a frequency of $f_{ac} = 1.90 \text{ MHz}$.

411 We mentioned and discussed many possible explanations for the light induced ejection
412 of particles in acoustic levitation. A plausible scenario seems to be the heating of the
413 surrounding fluid layer leading to instability mechanisms. To further clarify this hypothesis,
414 more experiments are needed, especially temperature controlled ones.

415 **VIII. CONCLUSION**

416 Choosing the proper geometric and acoustic parameters, it is possible to control the
417 aggregation process of micro particles using our in-house ultrasonic resonators. Once the
418 aggregates are formed, it is possible to keep them in acoustic levitation as long as desired.
419 The only way to break the aggregates is to turn off the ultrasounds. Nevertheless we show
420 that it is possible to destroy an aggregate of fluorescent particles just by illuminating it at
421 the proper absorption wavelength. This phenomenon depends on both the acoustic force
422 amplitude and the illumination power : the expulsion of the particles can only be observed
423 in acoustic levitation, suggesting a strong coupling between acoustics and photonics effects.
424 Above a given critical illumination power, the aggregate literally explodes. The expulsion
425 of the particles from the illuminated area can be very fast with an expulsion velocity which
426 depends on the injected power (acoustic amplitude and illumination power). Early observa-
427 tions also show that the phenomenon is affecting living cells such as red blood cells, opening
428 the path to many applications of these findings. This phenomenon, which may be named
429 *optoacoustophoresis* due to its dependence on both excitations, opens the path to many new
430 manipulations and sorting processes of suspensions, combining both acoustic and optical
431 properties of particles or cells. This new branch of acoustofluidics could be called *optoa-*

432 *coustofluidics*. The potential applications are numerous for both diagnosis or production,
433 such as fine cell separation for analysis or rare cell tagging in continuous flow systems.

434 **ACKNOWLEDGMENTS**

435 The authors are grateful to Ecole Doctorale Frontières du Vivant (FdV) Programme
436 Bettencourt for supporting G. Dumy's PhD thesis. The authors would also like to thank
437 L. Bellebon for his important contribution on the manipulation and analysis of the acoustic
438 energy of the resonators, and M. Mounaix for the lend of the optical power probe used for
439 light characterization.

440 **REFERENCES**

- 441 ¹W. T. Coakley and J. F. Spengler, "Analytical scale ultrasonic standing wave manipulation
442 of cells and microparticles," *Ultrasonics* **38**, 638–641 (2000).
- 443 ²J. Nilsson, M. Evander, B. Hammarström, and T. Laurell, "Review of cell and particle
444 trapping in microfluidic systems," *Analytica chimica acta* **649**, 141–157 (2009).
- 445 ³O. Dron and J.-L. Aider, "Varying the agglomeration position of particles in a micro-
446 channel using acoustic radiation force beyond the resonance condition," *Ultrasonics* **53**(7),
447 1280–1287 (2013).
- 448 ⁴J. Hulström, O. Manneberg, K. Dopf, H. M. Hertz, H. Brismar, and M. Wiklund, "Pro-
449 liferation and viability of adherent cells manipulated by standing-wave ultrasound in a
450 microfluidic chip," *Ultrasound in medicine and biology* **33**, 175–181 (2006).

451 ⁵L. Rayleigh Proc. R. Soc. London **36**, 10 (1883).

452 ⁶L. K. Zarembo, “Acoustic streaming,” High Intensity Ultrasonic Fields **85**, 137–199 (1971).

453 ⁷S. Nomura, K. Murakami, and Y. Sasaki, “Streaming induced by ultrasonic vibration in
454 water vessel,” Japanese journal of applied physics **39**(6), 3636–3640 (2000).

455 ⁸R. E. Apfel, “Acoustic radiation pressure - principles and application to separation sci-
456 ence,” Fortschritte der akustik 19–36 (1990).

457 ⁹W. König, “Hydrodynamisch akustisch untersuchungen vol. 1,” Annalen der physic und
458 chemie, neue folge **42**, 353–370 (1891).

459 ¹⁰L. Rayleigh, “On the pressure of vibrations,” The philosophical magazine **3**, 338–346
460 (1902).

461 ¹¹V. F. K. Bjerknes, *Fields of Force* (Columbia University Press, New York, 1906).

462 ¹²L. V. King, “On the acoustic radiation pressure on spheres,” Proceedings of the Royal
463 Society of London, Ser. A **147**, 212–240 (1934).

464 ¹³K. Yosioka and Y. Kawasima, “Acoustic radiation pressure on a compressible sphere,”
465 Acustica **5**, 167–173 (1955).

466 ¹⁴L. P. Gor’kov, “On the forces acting on a small particle in an acoustic field in an ideal
467 fluid,” Sov. Phys. **6**(9), 773–775 (1962).

468 ¹⁵A. A. Doinikov, “Theory of acoustic radiation pressure for actual physics,” Physical review
469 E **54**, 6297–6303 (1996).

470 ¹⁶T. Tuziuti, T. Kozuka, and H. Mitome, “Measurement of distribution of acoustic radiation
471 force perpendicular to sound beam axis,” Japanese journal of applied physics **38**, 3297–

472 3301 (1999).

473 ¹⁷S. M. Woodside, B. D. Bowen, and J. M. Piret, “Measurement of ultrasonic forces for
474 particle-liquid separations,” *AICHE journal* **43**, 1727–1736 (1997).

475 ¹⁸G. Whitworth, M. A. Grundy, and W. T. Coakley, “Transport and harvesting of suspended
476 particles using modulated ultrasound,” *Ultrasonics* **29**, 439–444 (1991).

477 ¹⁹O. Dron and J.-L. Aider, “Acoustic energy measurement for a standing wave in a micro-
478 channel,” *Europhysics Letters* **97**, 44011 (2012).

479 ²⁰D. Bazou, A. Castro, and M. Hoyos, “Controlled cell aggregation in a pulsed acoustic field,”
480 *Ultrasonics* **52**(7), 842 – 850 (2012) [http://www.sciencedirect.com/science/article/
481 pii/S0041624X12000200](http://www.sciencedirect.com/science/article/pii/S0041624X12000200) doi: <http://dx.doi.org/10.1016/j.ultras.2012.01.005>.

482 ²¹S. Gutiérrez-Ramos, M. Hoyos, and J. Ruiz-Suárez, “Induced clustering of escherichia coli
483 by acoustic fields,” *Scientific reports* **8**(1), 4668 (2018).

484 ²²S. C. Takatori, R. De Dier, J. Vermant, and J. F. Brady, “Acoustic trapping of active
485 matter,” *Nature communications* **7** (2016).

486 ²³A. Castro and M. Hoyos, “Study of the onset of the acoustic streaming in parallel
487 plate resonators with pulse ultrasound,” *Ultrasonics* **66**, 166–171 (2016) [http://www.
488 sciencedirect.com/science/article/pii/S0041624X15002747](http://www.sciencedirect.com/science/article/pii/S0041624X15002747) doi: [http://dx.doi.
489 org/10.1016/j.ultras.2015.10.019](http://dx.doi.org/10.1016/j.ultras.2015.10.019).

490 ²⁴J. T. Karlsen, P. Augustsson, and H. Bruus, “Acoustic force density acting on inhomoge-
491 neous fluids in acoustic fields,” *Physical review letters* **117**(11), 114504 (2016).

492 ²⁵A. Regazzetti, M. Hoyos, and M. Martin, “Experimental evidence of thermophoresis of
493 non-Brownian particles in pure liquids and estimation of their thermophoretic mobility,”
494 The Journal of Physical Chemistry B **108**(39), 15285–15292 (2004).

495 ²⁶A. Garcia-Sabaté, A. Castro, M. Hoyos, and R. González-Cinca, “Experimental study on
496 inter-particle acoustic forces,” The Journal of the Acoustical Society of America **135**(3),
497 1056–1063 (2014).

498 ²⁷A. Castro, and M. Hoyos, “Determination of the secondary Bjerknes force in acoustic res-
499 onators on ground and in microgravity conditions,” Microgravity Science and Technology
500 **28**(1), 11–18 (2016).

501 ²⁸K. Yasuda, and T. Kamakura, “Acoustic radiation force on micrometer-size particles.,”
502 Applied physics letters **71**(13), 1771-1773 (1997).